Computational Materials Science 187 (2021) 110054

Contents lists available at ScienceDirect

Computational Materials Science

journal homepage: www.elsevier.com/locate/commatsci

Fully resolved strain field of the β'' precipitate calculated by density functional theory

Jonas Frafjord [a,b,*], Stéphane Dumoulin [a,c], Sigurd Wenner [c], Inga G. Ringdalen [a,c], Randi Holmestad [a,b], Jesper Friis [a,c]

[a] Centre for Advanced Structural Analysis (CASA), Norwegian University of Science and Technology (NTNU), N-7491 Trondheim, Norway
[b] Department of Physics, NTNU, Høgskoleringen 5, NO-7491 Trondheim, Norway
[c] SINTEF Industry, P.O.Box 4760 Torgarden, NO-7465 Trondheim, Norway

ARTICLE INFO

Keywords:
Aluminium alloy
β'' precipitate
Strain
Density functional theory
Transmission electron microscopy

ABSTRACT

The β'' precipitate is the main hardening phase in age hardenable Al-Mg-Si alloys, and it is therefore of major scientific and industrial importance. A full model of the β'' precipitate cross-section embedded in an aluminium host lattice is created for a range of precipitate sizes, and relaxed by first principle calculations. The influence of periodic images is avoided by applying a cluster based model with fixed boundary conditions, where the surface is corrected by a displacement field calculated by linear elasticity theory. The calculated misfit values between the precipitate and the host lattice vectors are consistent with experimental scanning transmission electron microscopy results. The misfit area increases proportionally with the cross sectional area, suggesting that the lattice parameters of β'' do not change as the size increases. Both the displacement field and the strain field are in agreement with experimental results. The strain field calculated by density functional theory shows a local zone close to the precipitate where the chemical contribution to the strain field is dominant. The strong correspondence between the experimental and the modelling results supports the methodology to be used in general to study other phases.

1. Introduction

Precipitation hardening is the main mechanism responsible for increase in the mechanical strength of the age-hardenable 6xxx-series of aluminium (Al) alloys, for which magnesium (Mg) and silicon (Si) are the main alloying elements. The 6xxx-series are widely used in industry, due to the high strength-to-weight ratio in combination with good extrudability. The high mechanical strength for this alloy series is typically reached by a large number density of the metastable β'' precipitates.

The precipitation sequence of the 6xxx-series has been investigated by using transmission electron microscopy in several studies [1–4]. The β'' precipitates are formed early in the precipitation sequence, grow as needles elongated in the $\langle 001 \rangle_{Al}$ crystallographic directions, and are coherent with minor misfit relative to the surrounding Al host lattice. The misfit generates a strain field around the precipitate that affects the interaction between the precipitate and other defects, such as solutes and dislocations [5].

Finding a reliable and efficient way of calculating the strain field near the interface between the Al host lattice and the β'' precipitate has been attempted by various authors. Ehlers et al. [6,7] calculated the strain field by combining linear elasticity theory (LET) and density functional theory (DFT). To circumvent the asymmetric strain field of the precipitate, different pieces of the interface were separately relaxed by DFT. The pieces were then stitched together to form the full strain field. They concluded that the strain field calculated by LET is a good initial guess. Ninive et al. [8] conducted full DFT calculations of models containing β'' embedded in the aluminium matrix using periodic boundary conditions. A consequence of the small simulation box combined with periodic boundary conditions was a high concentration of precipitates, which could yield non-physical ionic and electronic corrections.

The strain field surrounding β'' has also been studied experimentally [9,10]. Wenner et al. [9] mapped the displacement and strain fields of

* Corresponding author at: Centre for Advanced Structural Analysis (CASA), Norwegian University of Science and Technology (NTNU), N-7491 Trondheim, Norway.
E-mail address: Jonas.Frafjord@ntnu.no (J. Frafjord).

https://doi.org/10.1016/j.commatsci.2020.110054
Received 29 July 2020; Received in revised form 3 September 2020; Accepted 4 September 2020
Available online 24 October 2020
0927-0256/© 2020 The Author(s). Published by Elsevier B.V. This is an open access article under the CC BY license (http://creativecommons.org/licenses/by/4.0/).

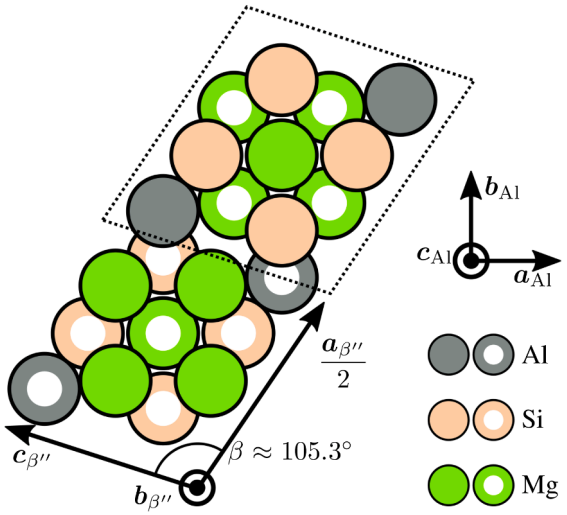

Fig. 1. Atomic model of the β'' precipitate. The unit cell consists of two formula units called eyes, one of which is marked by a stippled rhomboid. The open circles are the atoms in the lower plane, while the full circles are the atoms in the upper plane. $\boldsymbol{a}_{Al}$, $\boldsymbol{b}_{Al}$ and $\boldsymbol{c}_{Al}$ are the lattice vectors in Al, while $\boldsymbol{a}_{\beta''}$, $\boldsymbol{b}_{\beta''}$ and $\boldsymbol{c}_{\beta''}$ are the lattice vectors in the β'' precipitate.

the β'' precipitate by scanning transmission electron microscopy (STEM), and from the post-processing they were able to calculate the misfit values related to the precipitate lattice vectors. The misfit values were calculated for a range of precipitate sizes and showed that the relative misfit ratios varied based on the aspect ratio of the precipitate.

The main focus of this work is to calculate the misfit and strain field of the β'' with accuracy achievable by DFT but without the bias introduced by periodic boundary conditions. The challenge imposed by the periodic boundary conditions of plane-wave DFT is circumvented by a cluster based model, where the atoms in the fixed boundary are displaced by LET. An additional aim is to establish the approach as a general procedure that can be used to study other phases as well. The results presented by Wenner et al. [9] are used as a benchmark for this investigation, and previous numerical studies are discussed. In addition, the displacement and strain fields obtained from DFT and LET calculations are compared with those obtained by analysis of STEM images. This quantitative comparison is used to validate the methodology. The investigation in this work will add insight to the precipitate phase, and explore the cluster model approach to this problem. An accurate framework for calculating strain fields from first principles would be a step closer to develop a multi-scale framework for alloy design.

2. Background

The atomic structure and composition of β'' have been explored in several studies [11,12,8,2,13], and different chemical compositions have been investigated. From energy-dispersive X-ray spectroscopy [13] and DFT results [8] it was concluded that the most energetically favourable composition is $Mg_5Al_2Si_4$, which will be used in this work. The unit cell is illustrated in Fig. 1, with the relevant lattice vectors. The precipitate is monoclinic with $\beta = 105.3°$ [1]. Note that the unit cell contains two formula units that are symmetry related by the mirror plane perpendicular to the $\boldsymbol{b}_{\beta''}$ direction. All precipitates consist of a whole number of formula units in the plane defined by $\boldsymbol{a}_{\beta''}$ and $\boldsymbol{c}_{\beta''}$. The size of the precipitate is therefore described by the number of formula units, known as 'eyes'. For instance, a 3x4 precipitate has side lengths $L_a^{3x4} = \frac{3}{2}L_a = \frac{3}{2}|\boldsymbol{a}_{\beta''}|, L_c^{3x4} = 4L_c = 4|\boldsymbol{c}_{\beta''}|$ and is periodic in the $\boldsymbol{b}_{\beta''}$ direction. Fig. 1 also shows the relationship between the precipitate unit vectors and the Al unit vectors. The β'' unit vectors are given by

$$\boldsymbol{a}_{\beta''} = (1 + m_a)(2\boldsymbol{a}_{Al} + 3\boldsymbol{b}_{Al}) \tag{1a}$$

$$\boldsymbol{b}_{\beta''} = (1 + m_b)\boldsymbol{c}_{Al} \tag{1b}$$

$$\boldsymbol{c}_{\beta''} = (1 + m_c)(-3\boldsymbol{a}_{Al} + \boldsymbol{b}_{Al}), \tag{1c}$$

where m_a, m_b and m_c are the misfit parameters. The misfit along the needle direction, m_b, is small and therefore neglected in the DFT calculations in this investigation. In 2D, the misfit area is the additional cross-sectional area the precipitate occupies, as compared to no misfit.

The misfit values in Eq. (1) can be calculated by analysing the lattice vectors of the β'' precipitate. The average lattice vector is calculated by identifying the longest lattice vector, in the respective direction, between each identical atomic site in the precipitate and calculating the misfit using (1). The average misfit derived from all the atoms in the precipitate is used as the calculated misfit value.

Strain is a continuum scale quantity and is defined as the gradient of the displacement field, where both the direction of the gradient and the direction of the displacement field must be defined. To get an accurate description of the strain field for an atomic scale model, a discrete atomistic strain field must be defined. The interface between β'' and the Al matrix is coherent for small precipitates, simplifying the task of finding the displacement field in the vicinity of the interface. The displacement field, $\boldsymbol{U} = (U_i, U_j, U_k)$, is simply the deviation of the Al atoms from their respective lattice points in an underlying perfect lattice defined by the relaxed aluminium lattice constant. The subscript represents a specification to the direction. The strain is written as

$$\epsilon_{ij} = \frac{1}{2}\left(\frac{\partial U_j}{\partial x_i} + \frac{\partial U_i}{\partial x_j}\right), \tag{2}$$

and includes both shear and normal strain. For simplification, a central difference scheme is used to perform the differentiation. Using the central difference method, the normal strain can be expressed as

$$\epsilon_{ii} = \frac{\boldsymbol{a}_i^* - \boldsymbol{a}_i}{\boldsymbol{a}_i}, \tag{3}$$

where $\boldsymbol{a}_i^*$ is the strained lattice vector and $\boldsymbol{a}_i$ is the unstrained lattice vector. Note that ϵ_{xx}, ϵ_{yy}, ϵ_{aa} and ϵ_{cc} are the strain in the a_{Al}-, b_{Al}-, $a_{\beta''}$- and $c_{\beta''}$-directions, respectively.

3. Method and model

The DFT calculations are performed using the Vienna Ab Initio Simulation Package (VASP) [14,15]. The functional used for the calculations is the Perdew-Burke-Ernzerhof generalized gradient approximation [16], which has shown to be accurate for metals and is relatively computationally efficient. The plane-wave energy cut-off was 400 eV and a gamma sampling of k-points, with maximum distance of 0.18 $Å^{-1}$, was used to model the Brillouin zone. The k-point density was consistent for all calculations, and an independent sensitivity analysis of the k-point distance was done for bulk β'' and Al with consistent results. The bulk fcc Al lattice constant was found to be 4.046 Å by an initial DFT relaxation of bulk Al. The bulk values of the β'' precipitate are found through periodic bulk calculations of the β'' phase.

Defects in crystal structures are often accompanied by an asymmetrical strain. This asymmetry imposes a challenge when modelling defects with periodic plane-wave DFT, since the strain field surpasses the boundaries of the system. With periodic boundary conditions, the system has to be large enough for the stress field to be negligible at the boundaries, or the model must be designed in such a way that the stresses at the boundaries are cancelled. Alternatively, the system could be modelled with non-periodic boundaries to avoid the effect of the periodic images, e.g. by applying a cluster model for dislocations as explained in the review by Rodney et al. [17]. In it's simplest form, the

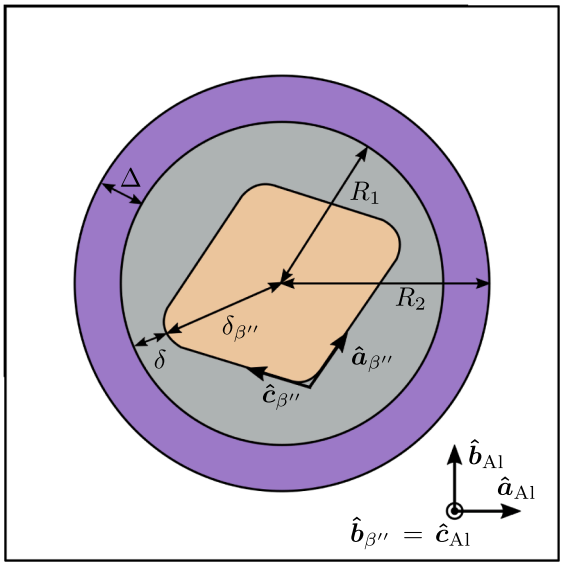

Fig. 2. A schematic illustration of the cross-section model of the β'' precipitate, coloured in orange, surrounded by a cylindrical Al slab represented by gray and purple. The atoms in the purple region are displaced by an elastic displacement field and held fixed during relaxation. R_1 is the radius of the relaxed region. $\Delta = R_2 - R_1$ is the width of the fixed region. δ is the shortest distance between the precipitate and the fixed region, while $\delta_{\beta''}$ is the remaining distance to the centre of the precipitate. $\hat{\boldsymbol{a}}_{\mathrm{Al}}$, $\hat{\boldsymbol{b}}_{\mathrm{Al}}$ and $\hat{\boldsymbol{c}}_{\mathrm{Al}}$ are the unit vector directions in Al, while $\hat{\boldsymbol{a}}_{\beta''}$, $\hat{\boldsymbol{b}}_{\beta''}$ and $\hat{\boldsymbol{c}}_{\beta''}$ are the unit vector directions in the β'' precipitate. The slab is one unit vector thick and periodic in the $\hat{\boldsymbol{c}}_{\mathrm{Al}}$ direction. The white region is the surrounding vacuum.

cluster model is surrounded by vacuum in the non-periodic directions, creating a free surface. The atoms in this surface must be corrected by a displacement field, and then constrained during relaxation. This creates a fixed region, where the width ensures that the atoms in the inner region are unaffected by the free surface, and react as if the atoms are enclosed by an infinite matrix containing an isolated defect. An accurate model is recognised by a displacement field that has a smooth transition from the relaxed region to the fixed region.

The atomic cluster model adapted in this work is illustrated in Fig. 2. The outer region is held fixed during relaxation of the inner region. The radius of the inner region is given by $R_1 = \delta + \delta_{\beta''}$, where δ is the shortest distance between the fixed region and the precipitate, and $\delta_{\beta''}$ is the remaining distance to the centre of the precipitate as illustrated in Fig. 2. δ is assumed to be independent of the precipitate size, and based on cluster size tests it was determined to be 6.5 Å. In agreement with the previous investigation of an edge dislocation [18], it was found that the width of the fixed region, $\Delta = R_2 - R_1$ had to be at least 6 Å. The model is periodic along the needle direction, with a slab thickness of one unit vector $|\boldsymbol{c}_{\mathrm{Al}}| = |\boldsymbol{b}_{\beta''}| = 4.046$ Å.

The displacement field superimposed on the Al atoms surrounding the precipitate depends on both the size and the aspect ratio of the precipitate. The displacement field can be separated in a chemical part and an elastic part. The former is mainly contributing to the strain field close to the precipitate, while the latter defines the long-range, geometrical effect. The long-range displacement field can be calculated from linear elastic theory (LET), by using the finite element method (FEM). This approach has been used in a previous investigation by Ehlers et al. [6] where Eshelby's methodology for inclusions [19] is followed. First, the precipitate is removed from the host lattice and relaxed to its bulk structure. Secondly, in order to fit the precipitate back into the hole in the Al host lattice, a compressive displacement field is applied to the precipitate. The internal surface of the host lattice and the external surface of the precipitate are then bonded together to ensure fully coherent interfaces. Lastly, the full system is relaxed. Note that simulations are performed for the second and third step, while the first step is imaginary. All elastic constants used in this procedure were determined from DFT studies of the isolated subsystems, see the work by Ehlers et al. [7] for further details. The FEM calculation results in an elastic displacement field that is dependent on the aspect ratio of the precipitate and scaled by the actual size of the precipitate. The results of the FEM calculations were superimposed to all atoms in the slab before constraining the atoms in the fixed region.

The experimental results were obtained from scanning transmission electron microscopy (STEM) images acquired with a double-corrected JEOL ARM-200F microscope, operated at an acceleration voltage of 80 kV. Images were distortion-corrected using Smart Align [20] and analysed with geometric phase approximation (GPA) [21] to extract displacement and strain fields. A plugin to the DigitalMicrograph software from HREM Research was used to perform the GPA calculation, where the chosen mask gives a spatial resolution of 8 Å. A more detailed description of the experimental method can be found in [9].

4. Results & discussion

4.1. Misfit

The calculated misfit values for the β'' bulk structure with periodic boundary conditions are $m_a = 5.1\%$, $m_b < 1\%$ and $m_c = 5.8\%$, indicating that the lattice vectors of the precipitate are longer than the corresponding lattice vector of Al. Thus, it is expected that the precipitate will be compressed when embedded in the Al matrix. Note that the constraint in the $\boldsymbol{b}_{\beta''}$-direction in the model with β'' embedded in the Al host lattice, might result in a slightly larger misfit in the remaining two directions. However, it is not expected to affect the final result significantly since m_b is small compared to the misfit in the two other directions. The calculated misfit values for the different sized β'' precipitates are summarised in Table 1, along with data from other selected studies [9,11,6,22]. The results show that the misfit of β'' is reduced compared to the Al bulk values when inserted into the

Table 1
Summary of the misfit values calculated in this work, along with values collected from different investigations. N_a and N_c are the number of β''-precipitate eyes in the $\boldsymbol{a}_{\beta''}$ and $\boldsymbol{c}_{\beta''}$ directions, respectively. m_a and m_c are the misfit value [%] in the $\boldsymbol{a}_{\beta''}$ and $\boldsymbol{c}_{\beta''}$ directions, respectively. The values in parenthesis are the difference between the calculated values in this work and the values collected from the respective study.

Size	DFT [this work]		ADF-STEM [9]		DFT[6]		DFT[11]		DFT [22]	
$N_a \times N_c$	m_a	m_c	m_a	m_c	m_a	m_c	m_a	m_c	m_a	m_c
Bulk	5.08	5.76					4.91	5.85	6.15	5.25
2×2	3.21	4.89								
3×3	3.30	4.56								
4×4	3.34	4.38	3.66 (0.32)	4.29 (−0.09)	2.45 (−0.89)	3.07 (−1.31)				
4×5	3.63	3.88	3.59 (−0.04)	3.36 (−0.52)						
5×3	2.59	5.40	2.62 (0.03)	4.54 (−0.86)						
5×4	3.01	4.74	3.09 (0.08)	4.61 (−0.13)						
5×5	3.32	4.27	3.36 (0.04)	3.69 (−0.58)						

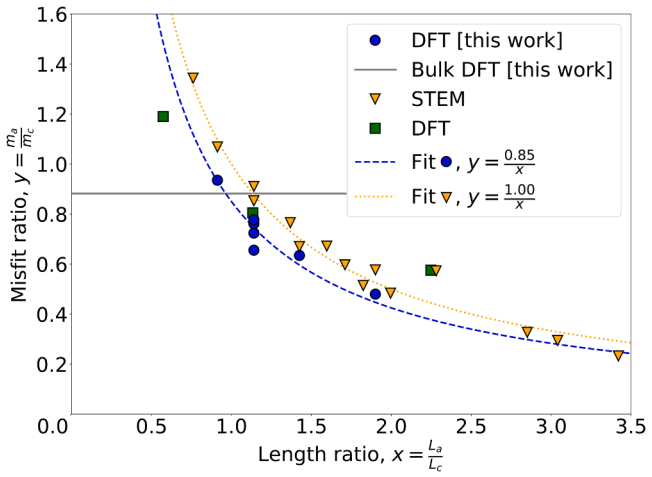

Fig. 3. The misfit ratio as a function of the length ratio of the β'' precipitate. The blue dots are results from this investigation, while the yellow triangles and green squares are data from Wenner et al. [9] and Ehlers et al. [22], respectively. The horizontal solid line represent the bulk misfit ratio calculated in this study. L_a and L_c are the length of the β'' interface in the $\boldsymbol{a}_{\beta''}$ and $\boldsymbol{c}_{\beta''}$ direction.s, respectively.

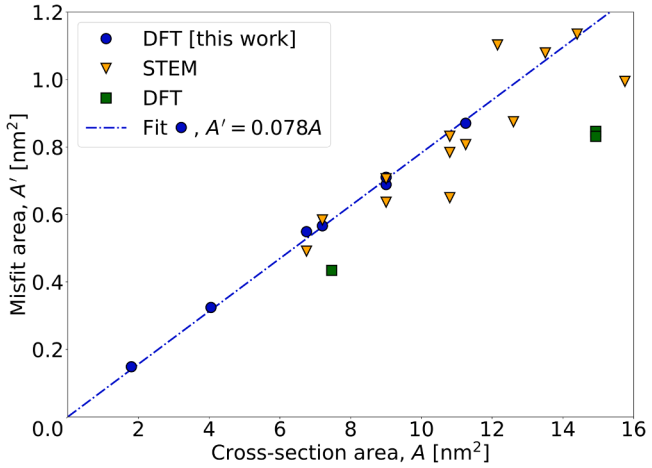

Fig. 4. The misfit area as a function of the cross-section area of the β'' precipitate. The blue dots are results from the present investigation. The line is a linear fit to the DFT results from this work.

aluminium lattice. The misfit values in the $\boldsymbol{c}_{\beta''}$ direction, m_c, are consistently larger than the corresponding misfit values in the $\boldsymbol{a}_{\beta''}$ direction, m_a. This is also the case for the bulk misfit values calculated in this study, and is in agreement with the DFT investigation by Ehlers et al. [6]. Contrary, Hasting et al. [11] predicted a larger bulk m_a compared to m_c. There is a good agreement between the results calculated in this work, and the experimental values by Wenner et al. [9]. Note that for some precipitate sizes, the results for m_c are found to be larger than the corresponding experimental values.

The difference between m_a and m_c varies based on the aspect ratio of the β'' precipitate. This effect is illustrated in Fig. 3, where the misfit ratio, $\frac{m_a}{m_c}$, is plotted as a function of the precipitate length ratio, $\frac{L_a}{L_c}$. This observation can be tied to the Poisson effect, where a material expands or contracts in the direction perpendicular to the loading direction. A precipitate elongated in one direction, having an aspect ratio different than one, is unevenly strained. Thus the host Al matrix loads the precipitate sides differently, resulting in a different misfit ratio. The results in Fig. 3 indicate that the relative misfit ratio is inversely proportional to the relative length ratio of the precipitate, with a constant multiplier of 0.85. In contrast, Wenner et al. [9] found a constant multiplier closer to 1, which means that the misfit ratio of a particle would be inverted if the aspect ratio of the particle was inverted. The consequence of a constant multiplier < 1, is that $m_c > m_a$, for an aspect ratio of 1. The multi-scale investigation by Ehlers et al. [22] did not capture this inverse proportionality. The strength of their study was that the interface region was improved, but without considering the core of the precipitate. Thus, an accurate description of the core region should not be expected from their results. Note that the length ratio is not the same as the relative number of eyes, since the side lengths of the precipitate are different to each other. However, they are close enough so that the number of eyes gives an indication of the relative length ratio for small precipitates.

Fig. 4 shows how the misfit area increases proportionally to the cross-section area. This again indicates that the precipitate size does not change the lattice parameters of the β'' precipitate. As a result, the total misfit strain increases proportionally with the size of the precipitate until the matrix is unable to accommodate the precipitate without lowering the strain. The strain can be relieved by different mechanisms, e.g. creating a misfit dislocation, changing the precipitate-host interface or by chemical adjustments. A study on how large a precipitate must be for this to occur would be interesting, but is outside the scope of this investigation.

The results presented in Fig. 4 are in agreement with both the experimental data by Wenner et al. [9] and the LET/DFT method by Ehlers et al. [22]. The linear fit of the DFT data from this work yields a slope of 7.8%, which is very close to the experimental result of 7.2% [9] and slightly higher than the LET/DFT results of 5.5% [22]. The higher slope indicates that the misfit values are on average larger, which is also confirmed by Table 1.

The numerical data for the misfit values obtained in this investigation generally give a better fit to experimental results compared to previous numerical studies. This is attributed to the cluster model approach, where the challenge of a periodic boundary is circumvented. A recurring observation is that the misfit in the $\boldsymbol{c}_{\beta''}$ direction, m_c, is consistently larger than the experimental values by Wenner et al. [9]. This is most likely caused either by the numerical approach used in this investigation or it is due to the strain relieving mechanisms that a physical β'' precipitate has. The value of m_c could be affected by the model geometry of the fixed boundary conditions, or the constraint on the $\boldsymbol{b}_{\beta''}$ direction. The latter is less likely to make a significant contribution, but the former could have an effect on the results.

4.2. Displacement and strain

The misfit values give an averaged description of the strain field inside the precipitate. A more detailed analysis of the strain field outside the precipitate requires an accurate displacement field. Fig. 5 shows the radial displacement field, $\Delta R = \sqrt{\Delta \boldsymbol{a}_{\mathrm{Al}}^2 + \Delta \boldsymbol{b}_{\mathrm{Al}}^2}$ [1], of the 5×5 β'' precipitate. Fig. 5(a) has been calculated by DFT, while Fig. 5(b) is the GPA results from the STEM image in Fig. 5(c). The STEM image is cut and rotated from a larger STEM image, which is provided in the Supplementary information. Based on the contour lines in Fig. 5(a), the radial displacement field has an even transition from the DFT relaxed atoms to the fixed atoms. The most rapid change in the displacement field is around the Si atoms at the interface between the precipitate and the host Al atoms. The displacement field near the precipitate interface clearly shows the chemical contribution from the local variations around the different elements of the interface. This is not observed in the results from STEM since the GPA analysis has a spatial resolution of 0.8 nm. The spatial resolution could be increased by using a different mask in the Fourier space, but this would be at the expense of accuracy. The displacement field given by the experimental work is observed to be

[1] $\Delta \boldsymbol{a}_{\mathrm{Al}}$ and $\Delta \boldsymbol{b}_{\mathrm{Al}}$ are the displacement in $\widehat{\boldsymbol{a}}_{\mathrm{Al}}$- and $\widehat{\boldsymbol{b}}_{\mathrm{Al}}$-directions, respectively

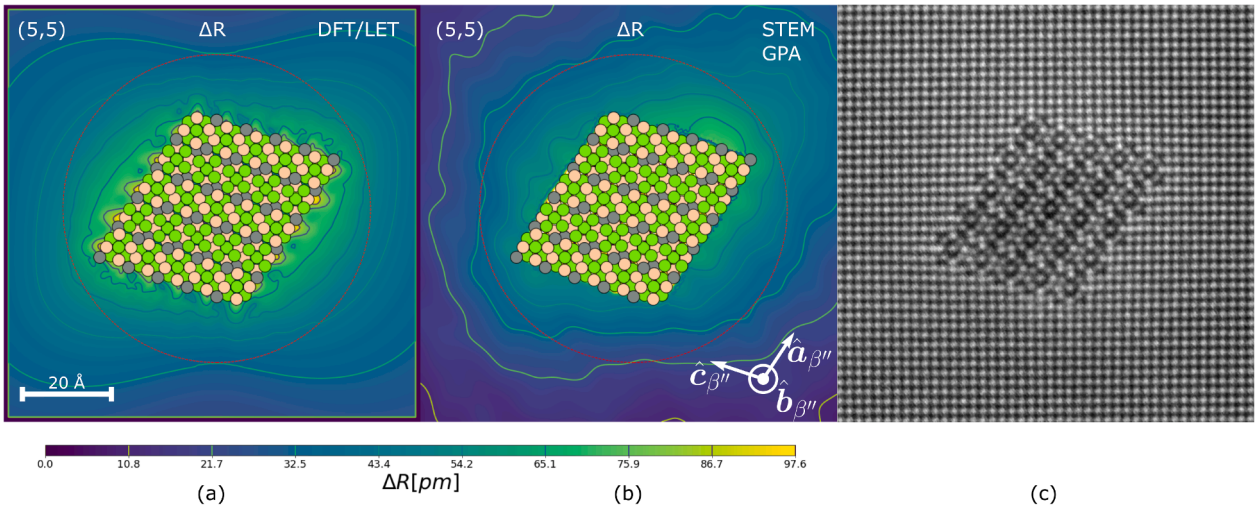

Fig. 5. The radial displacement field, ΔR, for a 5×5 β'' precipitate. (a) was calculated from atoms relaxed by DFT, inside the red circle, and atoms relaxed by LET, outside the red circle. (b) is the GPA result of the STEM image in (c). The blue bar is the scale bar, common for all subfigures. The coloured dots represent the precipitate, where the beige, lime and grey are Si, Mg and Al atoms, respectively.

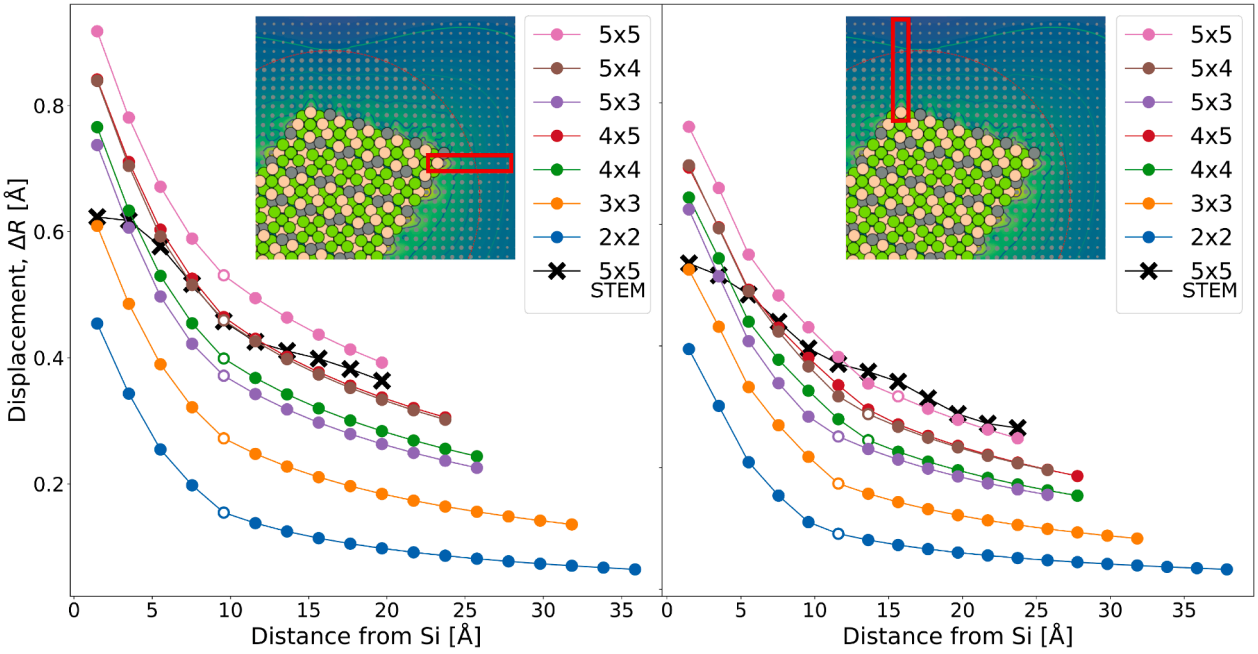

Fig. 6. Linescans of the displacement field for different sized β'' precipitates. The size description follows $N_a \times N_c$, representing the number of β'' eyes. The linescans are taken along the atoms marked by the red box. The coloured dots in the inset figure represent the precipitate, where the beige, lime and grey are Si, Mg and Al atoms, respectively. The open dots in the graph are the first atom outside the red circle, separating the DFT relaxed region, inside, and the LET relaxed region, outside. The black line with cross markers is GPA results from the STEM image shown in Fig. 5(c).

asymmetrical, which is most likely an artefact either caused by being slightly off the zone axis during scanning, or by the strain field of a defect outside the field of view of the STEM image. Since the precipitate is isolated in the numerical calculations, the displacement field is expected to be more symmetrical.

Fig. 6 shows graphs of linescans of the displacement field for the different precipitate sizes. The linescans are taken over the atoms marked by the red box in the figure, where the reference position is the Si atom at the interface. The displacement field displays a significant change in the gradient at the transition from the relaxed to the fixed region. This indicates that the chemical contribution is of short range, and contributes considerably to the displacement field near the interface. The experimental results fit well with the numerical data, except for the change in slope near the interface. The value of the displacement field near the interface, calculated by GPA, is inaccurate due to the limited spatial resolution of the technique, which causes the unphysical displacement field inside β'' to be part of the calculated value. The capture of the chemical contribution strengthens the assumption that δ is independent of the precipitate size. In addition, the displacement field shows a smoother transition from the DFT- to the LET-relaxed region for the larger precipitates, further supporting this assumption.

Ninive et al. [8] investigated the displacement field, and analysed its gradient, i.e. the rate at which it changed. They made an exponential fit to the displacement field, which was accurate for the smaller precipitates, but less accurate for the larger ones. They attributed this to be a defect caused by the system size. However, the GPA results presented

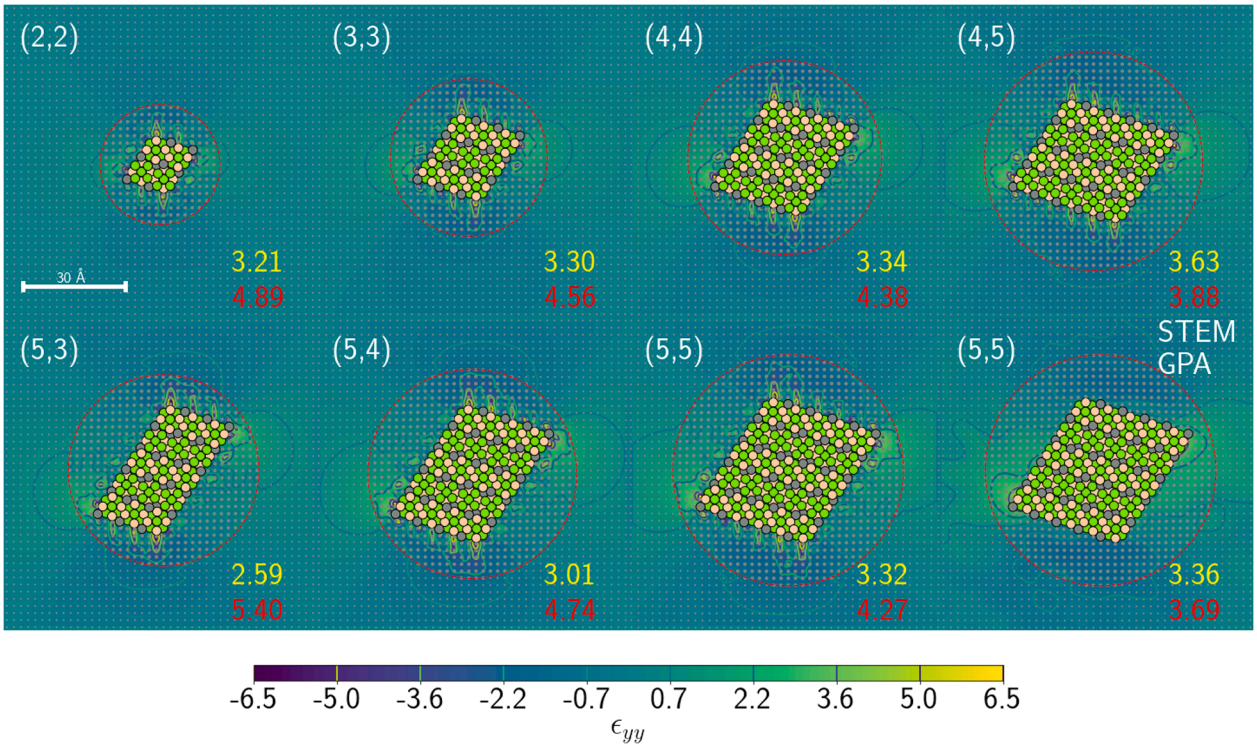

Fig. 7. The strain field, ϵ_{yy}, for different β''-precipitate sizes, indicated by (N_a, N_c), where N_a and N_c are the number of β'' eyes in the $\boldsymbol{a}_{\beta''}$ and $\boldsymbol{c}_{\beta''}$ directions, respectively. The subfigure in the lower right corner is GPA results of an experimental STEM image. The other subfigures are calculated from atomic positions relaxed by DFT, inside the red circle, and LET, outside the red circle. The small grey dots are the Al host matrix. The larger coloured dots represent the precipitate, where beige, lime and grey are Si, Mg, and Al atoms, respectively. The yellow upper number is m_a, and the red bottom number is m_c, where m_a and m_c are the misfit values in the $\boldsymbol{a}_{\beta''}$ and $\boldsymbol{c}_{\beta''}$ directions, respectively.

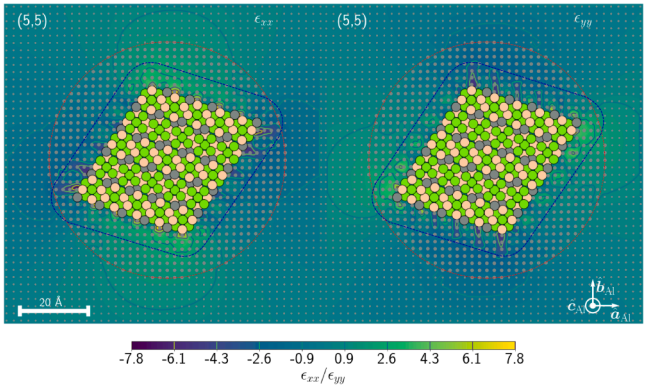

Fig. 8. The strain fields, ϵ_{xx} and ϵ_{yy}, for the 5×5 β''-precipitate. The small grey dots are the Al host matrix. The larger coloured dots represent the precipitate, where beige, lime and grey are Si, Mg, and Al atoms, respectively. The red circle separates the DFT-relaxed atoms, inside, and the LET-fixed atoms, outside. The blue box encloses the region where the chemical effect of the strain field is identifiable. m_a and m_c are the misfit values in the $\boldsymbol{a}_{\beta''}$ and $\boldsymbol{c}_{\beta''}$ directions, respectively.

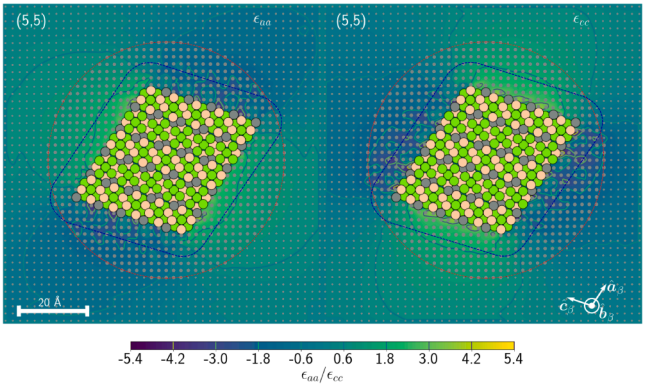

Fig. 9. The strain fields, ϵ_{aa} and ϵ_{cc}, for the 5×5 β''-precipitate. The small grey dots are the Al host matrix. The larger coloured dots represent the precipitate, where beige, lime and grey are Si, Mg, and Al atoms, respectively. The red circle separates the DFT-relaxed atoms, inside, and the LET-fixed atoms, outside. The blue box encloses the region where the chemical effect of the strain field is identifiable. m_a and m_c are the misfit values in the $\boldsymbol{a}_{\beta''}$ and $\boldsymbol{c}_{\beta''}$ directions, respectively.

in Fig. 5b) and the experimental results by Wenner et al. [9], indicate that the displacement field should be ~0.35 Å at 20 Å away from the precipitate [2], and that it decreased at a slower rate than the exponential fit predicted by Ninive et al. The displacement field from the larger precipitates should be higher due to the misfit area being proportional to the cross-section area. The Al atoms just outside the precipitate must be displaced equal to the misfit times the β'' size to accommodate the extra space which the particle occupies.

Fig. 7 shows the strain field, ϵ_{yy}, for all the analysed precipitate sizes. The features found in the strain maps are consistent for the different sizes. Thus, the following discussion will focus on the strain field resulting from the largest precipitate, with 5×5 β'' eyes. The strain maps for the remaining β'' sizes can be found in the Supplementary information. Note that the strain field in the lower right corner of Fig. 7 is the result of the GPA analysis of the STEM image in Fig. 5(c). The

[2] Fig. 1b in reference [9]

experimental results are in agreement with the numerical data, but does not have as high spatial resolution as obtained in the numerical work. Thus, the focus of the following discussion will be on the numerical calculations in order to evaluate the finer details in the strain maps which are not captured experimentally.

The strain fields ϵ_{xx} and ϵ_{yy} are presented in Fig. 8, and the strain fields ϵ_{aa} and ϵ_{cc} can be seen in Fig. 9. The general trend is that the strain field can be separated into two contributions. One of these is only observed close to the interface and the other dominates further away from the precipitate. The former is the chemical contribution, which can be observed inside the blue line in Figs. 8 and 9, where there are local variations due to the different chemical elements. Here, the strain field is concentrated near the Si atoms, with the extreme points closest to the interface. The latter is associated with the elastic field, where the geometry of the precipitate is more important than the chemical environment around the interface. This contribution is long range, and thus observed outside the blue line, where the strain field is typically $\epsilon < 1\%$.

The strain fields ϵ_{aa} and ϵ_{cc} show that the Al matrix is compressed in the respective directions as expected based on the positive misfit values. Since the bulk lattice vectors of β'' are larger than the Al ones, the Al atoms are compressed in the $\boldsymbol{a}_{\beta''}$ direction near the top and bottom interface, and stretched in the left and right interface. Consequently, the Al atoms are compressed in the $\boldsymbol{c}_{\beta''}$ direction near the left and right interface, and stretched in the top and bottom interface. There is a good agreement with the LET field and the DFT relaxed region, as the contour lines are smooth over the boundary to the fixed region, see Fig. 8 and 9.

5. Conclusion

Full models of different sized β'' precipitate cross-sections are relaxed by DFT using a cluster model approach. The precipitates are relaxed as isolated phases in an Al host lattice with a fixed outer layer and thereby avoiding the influence of periodic images. The misfit associated with the β'' precipitates are analysed, and found to be consistent with experimental results. The Poisson effect is observed, as the misfit ratio changes based on the aspect ratio of the precipitate. The analysis of different precipitate sizes shows that the misfit area is proportional to the cross-sectional area, indicating that the lattice parameters of β'' are not changed by the increased size of the precipitate. It follows that strain relieving mechanisms must occur at some point as the precipitate cross-section area increases. A fully resolved displacement field is presented, with accuracy achievable by DFT. A STEM image of the 5×5 precipitate is analysed, and GPA analysis of the displacement field is compared with the simulated result, showing good agreement between experiment and theory. This results in an accurately described strain field, where the elastic and the chemical contributions can be visually observed. A transition from where the two contributions dominate the strain field is indicated. As expected, the chemical contribution does not extend farther into the host matrix when the cross-sectional area increases.

Data availability

The raw data used to reproduce the presented results are available in the Zenodo repository, https://doi.org/10.5281/zenodo.3937494 [23].

CRediT authorship contribution statement

Jonas Frafjord: Methodology, Software, Investigation, Formal analysis, Writing - original draft. **Stéphane Dumoulin:** Methodology, Software, Writing - review & editing. **Sigurd Wenner:** Investigation, Writing - review & editing. **Inga G. Ringdalen:** Supervision, Writing - review & editing. **Randi Holmestad:** Supervision, Writing - review & editing. **Jesper Friis:** Methodology, Software, Supervision, Writing - review & editing.

Declaration of Competing Interest

The authors declare that they have no known competing financial interests or personal relationships that could have appeared to influence the work reported in this paper.

Acknowledgements

Sigurd Ofstad is acknowledged for creating the DFT supercell, for conducting and analysing the convergence tests and giving valuable insight to the numerical calculations.

The authors acknowledge the Centre for Advanced Structural Analysis (CASA), funded by the Research Council of Norway (RCN) [Grant No.: 237885] and its industrial partners. The computations were made possible due to resources provided by UNINETT Sigma2 - the National Infrastructure for High Performance Computing and Data Storage in Norway [Grant No.: NN8068K]. The STEM work was conducted on the NORTEM [RCN Grant No.: 197405] infrastructure at the TEM Gemini Centre, Trondheim, Norway.

Appendix A. Supplementary data

Supplementary data associated with this article can be found, in the online version, at https://doi.org/10.1016/j.commatsci.2020.110054.

References

[1] H.W. Zandbergen, S.J. Andersen, J. Jansen, Structure determination of Mg5Si6 particles in Al by dynamic electron diffraction studies, Science 277 (1997) 1221–1225.
[2] S.J. Andersen, H.W. Zandbergen, J. Jansen, C. Træholt, U. Tundal, O. Reiso, The crystal structure of the β'' phase in Al-Mg-Si Alloys, Acta Mater. 46 (9) (1998) 3283–3298.
[3] A.G. Frøseth, R. Høier, P.M. Derlet, S.J. Andersen, C.D. Marioara, Bonding in MgSi and Al-Mg-Si compounds relevant to Al-Mg-Si alloys, Phys. Rev. B 67 (2003), 224106.
[4] J.H. Chen, E. Costan, M.A. van Huis, Q. Xu, H.W. Zandbergen, Atomic pillar-based nanoprecipitates strengthen AlMgSi alloys, Science 312 (2006) 416–419.
[5] I. Ringdalen, S. Wenner, J. Friis, J. Marian, Dislocation dynamics study of precipitate hardening in Al-Mg-Si alloys with input from experimental characterization, MRS Commun. 7 (3) (2017) 626–633.
[6] F.J. Ehlers, S. Dumoulin, K. Marthinsen, R. Holmestad, Interface energy determination for the fully coherent β'' phase in Al-Mg-Si: making a case for a first principles based hybrid atomistic modelling scheme, Model. Simul. Mater. Sci. Eng. 21 (8) (2013).
[7] F.J. Ehlers, R. Holmestad, Ab initio based interface modeling for fully coherent precipitates of arbitrary size in Al alloys, Comput. Mater. Sci. 72 (2013) 146–157.
[8] P.H. Ninive, O.M. Løvvik, A. Strandlie, Density functional study of the β'' phase in Al-Mg-Si alloys, Metall. Mater. Trans. A 45 (6) (2014) 2916–2924.
[9] S. Wenner, R. Holmestad, Accurately measured precipitate-matrix misfit in an Al-Mg-Si alloy by electron microscopy, Scr. Mater. 118 (2016) 5–8.
[10] L. Jones, S. Wenner, M. Nord, P.H. Ninive, O.M. Løvvik, R. Holmestad, P.D. Nellist, Optimising multi-frame ADF-STEM for high-precision atomic-resolution strain mapping, Ultramicroscopy 179 (2017) 57–62.
[11] H.S. Hasting, A.G. Frøseth, S.J. Andersen, R. Vissers, J.C. Walmsley, C.D. Marioara, F. Danoix, W. Lefebvre, R. Holmestad, Composition of β'' precipitates in Al-Mg-Si alloys by atom probe tomography and first principle calculations, J. Appl. Phys. 106 (12) (2009).
[12] C. Ravi, C. Wolverton, First-principles study of crystal structure and stability of Al-Mg-Si-(Cu) precipitates, Acta Mater. 52 (14) (2004) 4213–4227.
[13] S. Wenner, L. Jones, C.D. Marioara, R. Holmestad, Atomic-resolution chemical mapping of ordered precipitates in Al alloys using energy-dispersive X-ray spectroscopy, Micron 96 (2017) 103–111.
[14] G. Kresse, J. Hafner, Ab initio molecular dynamics for liquid metals, Phys. Rev. B 47 (1) (1993) 558.
[15] G. Kresse, J. Furthmüller, Efficient iterative schemes for ab initio total-energy calculations using a plane-wave basis set, Phys. Rev. B 54 (16) (1996) 11169.
[16] J.P. Perdew, K. Burke, M. Ernzerhof, Generalized gradient approximation made simple, Phys. Rev. Lett. 77 (18) (1996) 3865–3868.
[17] D. Rodney, L. Ventelon, E. Clouet, L. Pizzagalli, F. Willaime, Ab initio modeling of dislocation core properties in metals and semiconductors, Acta Mater. 124 (2017) 633–659.
[18] J. Frafjord, I.G. Ringdalen, O.S. Hopperstad, R. Holmestad, J. Friis, First principle calculation on pressure dependent yielding in solute strengthened aluminium alloys, Comput. Mater. Sci. 184 (2020) 109902.
[19] J.D. Eshelby, R.E. Peierls, The determination of the elastic field of an ellipsoidal inclusion, and related problems, Proc. R. Soc. London Ser. A 241 (1957) 376–396.

[20] L. Jones, H. Yang, T.J. Pennycook, M.S. Marshall, S. Van Aert, N.D. Browning, M. R. Castell, P.D. Nellist, Smart Align—a new tool for robust non-rigid registration of scanning microscope data, Adv. Struct. Chem. Imag. 1 (1) (2015) 1–16.
[21] M.J. Hÿtch, E. Snoeck, R. Kilaas, Quantitative measurement of displacement and strain fields from HREM micrographs, Ultramicroscopy 74 (3) (1998) 131–146.
[22] F.J. Ehlers, S. Dumoulin, K. Marthinsen, R. Holmestad, Interfacial and strain energy analysis from ab initio based hierarchical multi-scale modelling: the Al-Mg-Si alloy β phase, Mater. Sci. Forum 794–796 (2014) 640–645.
[23] J. Frafjord, S. Dumoulin, S. Wenner, I.G. Ringdalen, R. Holmestad, J. Friis, Data for fully resolved strain field of the β'' precipitate calculated by density functional theory (2020).https://doi.org/10.5281/zenodo.3937494.